

SUPPLEMENTARY INFORMATION

Supplementary Materials

All study subjects were given an injection of radiotracer immediately prior to behavioral testing. Anesthesia, blood sample collection, and a PET scan followed behavioral testing. On a separate day a structural MRI was collected to aid in image registration. An anxious temperament composite (AT) was calculated for each animal and whole-brain regression analyses were performed to examine the relations between brain activity and AT. Each of these steps is described in detail below.

Subjects

240 monkeys (*Macaca mulatta*) underwent combined behavioral testing and FDG-PET scans. Two of the animal's data were unusable because of poor image quality. All animals were mother-reared, and pair-housed at the Harlow Primate Laboratory and the Wisconsin National Primate Research Center. At the time of behavioural testing/brain scans, the mean age was 2.4 years (range = 0.74 – 4.2 years), the median age was 2.34 years, there were only four animals that had reached the age of 4 years, and there were only nine animals less than 1 year of age. The typical life span of a rhesus macaque is approximately 25 years. Females reach puberty around three years old, and males reach puberty between three and 3.5 years of age (cf. Wisconsin Primate Research Center). This would correspond to a human sample of mostly prepubescent children with some peri-adolescents. A histogram demonstrating the age range of the animals used in the study is presented below in Supplementary Figure 1. Animal housing and experimental procedures were in accordance with institutional guidelines.

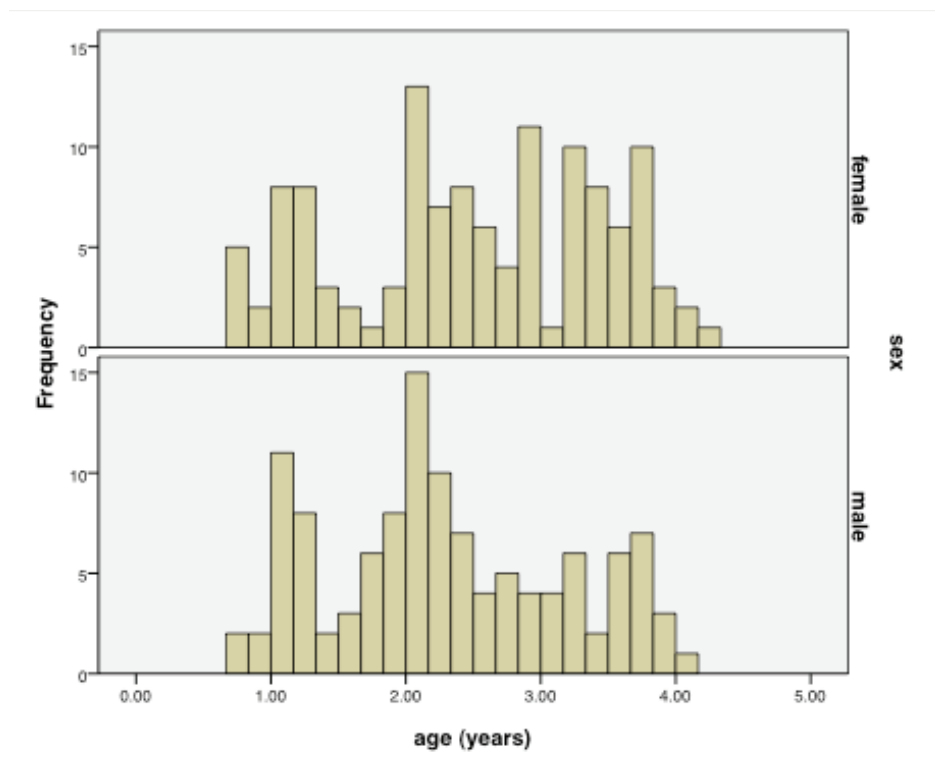


Figure S1. Histogram presenting the age range of male and female study subjects.

Fluoro-18-deoxyglucose PET Acquisition

The capturing of animals for testing was accomplished by having them voluntarily run into a transport cage. The capture procedure lasted less than two minutes in nearly all animals. The average time between capture and radiotracer injection was 6 minutes. Animals received intravenous injections of 10 mCi [^{18}F]-flouro-2-deoxyglucose (FDG) immediately before exposure to the 30-minute behavioral paradigm (described below), during which FDG-uptake occurred. After the behavioral paradigm, subjects were anesthetized with 15mg/kg ketamine intramuscularly for placement of an endotracheal tube and then positioned in a stereotactic head holder, and given isoflurane gas

anesthesia (1-2%) for the duration of the 60-minute scanning procedure, during which integrated FDG-uptake from the behavioral paradigm was measured. Scanning was performed using the microPET P4 scanner (Concorde Microsystems, Inc., Knoxville, TN), which has an approximate resolution of 8mm³.

Behavioral Paradigm

Each monkey was injected with FDG immediately preceding the No Eye Contact (NEC) challenge. During the experimental paradigm, FDG-uptake occurred and behaviors were monitored non-invasively. During NEC the animals were placed in a test-cage and a male human (the “intruder”) entered the room and stood still at a distance of 2.5 meters presenting his profile to the animal. Following 30-minutes of exposure to the experimental condition, animals were anesthetized and blood samples were taken.

Behavioral Assessment

During the NEC challenge behavior was assessed using standard methods by a trained rater using a closed-circuit television system. Freezing was defined as a period of at least 3 seconds characterized by tense body posture, no vocalizations, and no locomotion except for slow movements of the head. Coo vocalizations were defined as audible calls made by rounding and pursing the lips with an increase then decrease in frequency and intensity. To ensure that behavioral data were normally distributed, the duration of freezing behavior was log-transformed and the frequency of coo vocalizations was square root transformed. Cortisol was measured in plasma samples

using an enzyme immunoassay kit as described below. To create the composite measure of AT, we first calculated the inverse of cooing frequency since reduced cooing is associated with increased anxiety in the NEC condition. Using SPSS each measure (freezing, cortisol, and cooing) was run in a linear regression model to remove any variance associated with age (and time of day for cortisol sampling) and saved as standardized residuals. The mean of the three z-scored measures was then computed for each subject. For additional details on the composite measure of AT, see reference 2 in the Letter.

Cortisol Assay

Plasma was immediately separated from whole blood by centrifugation for 10 minutes at 1,900 x g at 4°C and frozen at –70°C until assayed. Cortisol was measured in duplicate in plasma samples using the Diagnostic Products Corporation Coat-A-Count cortisol radioimmunoassay (Siemens Medical Solutions Diagnostics, Los Angeles, CA). The inter-assay CV was 6.6%, and the detection limit was defined as the lowest standard used in the assay, 1.0 µg/dL.

MRI Scanning

Magnetic resonance imaging (MRI) data were collected using a GE Signa 3T scanner (General Electric Medical Systems, Milwaukee, WI) with a standard quadrature birdcage headcoil using an axial 3D T1-weighted inversion-recovery fast gradient echo sequence (repetition time, 9.4 ms; echo time, 2.1 ms; field of view, 14 cm; flip angle, 10°; number

of excitations, 2; in-plane resolution, 0.2734 mm; number of slices, 248; slice thickness, 1 mm; -0.05 mm interslice gap). Before undergoing MRI acquisition, the monkeys were anesthetized with an intramuscular injection of ketamine (15 mg/kg). Structural MRI data were collected within as close temporal proximity of PET/behavioral data collection as possible.

FDG-PET Pre-Processing

Using standard methods, each subject's anatomical image was transformed to the stereotaxic space of Paxinos, Huang, Petrides & Toga³¹ after the creation of a study-specific template. First, each subject's T1-MRI image was manually striped of non-brain tissue using SPAMALIZE; http://brainimaging.waisman.wisc.edu/~oakes/spam/spam_frames.htm. Brain extracted MRI images were registered to a 34-brain template (see reference 2 in the Letter) in standard space, using a 12-parameter linear transformation with FMRIB Software Library's "flirt" tool (FSL; <http://www.fmrib.ox.ac.uk/fsl/>)³². Images were manually verified, and averaged to create a study-specific 238-brain template in standard space. The brain-extracted MRI images in original space were then transformed to match this study-specific template using non-linear transformation tool in FSL ("fnirt"). In addition to a study-specific template, this procedure resulted in transformations from each subject's original T1-MRI to standard space. The T1 images in standard space were segmented into the probability of gray matter, white matter and cerebrospinal fluid while also correcting for RF inhomogeneities using FSL ("fast"). The underlying method is based on a hidden Markov random field model and an associated Expectation-Maximization

algorithm; <http://www.fmrib.ox.ac.uk/fsl/fast4/index.html>³³. This procedure resulted in a subject-specific probability map, in which each point represented the probability of gray matter at each voxel in standard space. Each animal's FDG-PET image was coregistered to its T1-MRI image in native space using a 6-parameter linear transformation, and these transforms were combined with the MRI->template transforms. The combined transformations (PET->MRI->template) were applied to the original FDG-PET images. The coregistered FDG-PET image intensities were scaled to the global mean FDG signal across the entire brain to allow for across subject comparison. Both the scaled FDG-PET images and gray-matter probability maps were smoothed using a 4mm Full Width Half Max (FWHM) Gaussian smoothing kernel to further facilitate across subject statistical comparisons.

Regression Analyses

Statistical analyses were performed using an adapted version of Fmristat; <http://www.math.mcgill.ca/keith/fmristat/>^{34,35}. The regression analyses were performed across the whole-brain while controlling for age, sex and the probability of gray-matter on a voxelwise basis; <http://brainimaging.waisman.wisc.edu/~fox/multistatic/>. This allowed analyses to be controlled for gross anatomical differences and registration error³⁶. The results of the voxelwise regression analysis were corrected for multiple comparisons using the Šidák equation, which is similar to the Bonferroni method. The equation for the calculation of the corrected p value is as follows, $1 - (1 - \alpha)^{1/n}$, where $\alpha = 0.05$, and $n =$ the number of tests (i.e., voxels in the brain, which was = 435882). This determined the corrected α level to equal $p = 0.00000005875$, which corresponded to a

t-statistic = 5.4671. Only those clusters that were larger than the minimum scanner resolution were considered for further study. For graphic representation of the significance of the correlations (see Fig 1 in the Letter), we calculated the corrected p value for three increasingly conservative levels of α ($p = 0.05$, $t = 5.47$; $p = 0.01$, $t = 5.79$; and $p = 0.001$, $t = 6.22$). Results did not change when gray matter probability was removed as a covariate from the voxelwise analyses, further confirming the lack of influence of any gray matter differences on the relation between metabolic activity and AT.

Calculating the 95% Spatial Confidence Intervals

Spatial confidence intervals around the voxels containing the maximally significant correlations between metabolic activity and AT were calculated using the program *conf_region*, which is part of *fmrstat*³⁷. The confidence intervals were defined as contiguous voxels with $t \geq \sqrt{(\text{peak}_t)^2 - \chi^2_3(.05)}$;
<http://www.math.mcgill.ca/keith/fmrstat/#confregion>.

5-HTT Availability Map

The [¹¹C]DASB-PET methods are detailed elsewhere³⁸, and are only briefly described here. DASB is a high-affinity ligand of 5-HTT, and the carbon-11 for the radiolabeling was produced with a National Electrostatics 9SDH 6 MeV Van de Graff tandem accelerator (Middleton, WI). PET data were acquired in 34 rhesus monkeys (mean age = 4.4 years; 12 male, 22 female) using a Concorde microPET P4 scanner³⁹. The

dynamic PET time series were transformed into parametric images with each voxel representing the distribution volume ratio (DVR) serving as an index of receptor binding⁴⁰. The cerebellum was used as a reference region, and all voxels were divided by the mean cerebellar binding values. Each subject's DVR image was transformed into standard space based on the corresponding MRI transformation. The group-averaged 5-HTT map was thresholded at 250x background cerebellar binding and used to demarcate the location of the lateral division of the CeA.

Assessment of Possible Laterality and Sex Differences, and the Effects of Age

We did not observe any effects of sex on the components used to derive anxious temperament (freezing duration, vocalizations, and cortisol concentration). There was a small but significant difference between males and females in the unresidualized mean FDG signal extracted from the 95% confidence intervals most predictive of AT. We also observed significant correlations between age and the components of the AT composite, and there were also significant correlations between age and the mean FDG signal in the hippocampal and amygdala 95% confidence intervals most predictive of AT. This information is presented in supplementary Table S1 (below). We controlled for the potential influences of age and sex in all of our analyses, and residualized the components used to derive anxious temperament for the effects of age before calculating the composite. Possible differences in the correlations between AT and glucose metabolism across hemisphere were analyzed by extracting the corresponding voxels in the opposite hemisphere from those reported in the paper (i.e., the

corresponding left dorsal amygdala voxel and the corresponding right anterior hippocampus voxel) and testing the difference between two dependent correlation coefficients⁴¹. Possible sex differences in the reported correlations between AT and glucose metabolism were analyzed by testing the difference between two independent correlation coefficients⁴¹. No effects of sex or laterality were observed in any of the reported correlations (all p 's > 0.10), nor were there any significant sex by AT interactions on glucose metabolism (FDR, q > 0.05).

Supplementary Table 1

MAIN EFFECTS OF SEX

variable	mean for males	mean for females	t-stat	Sig. (2-tailed)
freezing (sec per 5min)	36.25	32.99	t = 0.439	p = 0.661
coo calls (frequency)	11.25	14.43	t = -1.023	p = 0.094
cortisol ($\mu\text{g}/\text{dL}$)	67.35	64.34	t = 1.398	p = 0.163
hipp FDG (arbitrary units)	3.816	3.706	t = 3.246	p = 0.001
amyg FDG (arbitrary units)	3.657	3.583	t = 2.436	p = 0.016

MAIN EFFECTS OF AGE

variable	Pearson's r	Sig. (2-tailed)
freezing (sec per 5min)	0.206	p = 0.001
coo calls (frequency)	-0.399	p < 0.001
cortisol ($\mu\text{g}/\text{dL}$)	-0.621	p < 0.002
hipp FDG (arbitrary units)	-0.13	p = 0.044
amyg FDG (arbitrary units)	-0.272	p < 0.001

Table S1. (Top) No significant effects of sex were observed on the components of AT. Glucose metabolism was slightly, but significantly higher in males than in females in the regions most strongly correlated with AT. (Bottom) Significant correlations between age and the components of AT, as well as glucose metabolism in the regions most strongly correlated with AT were observed.

Genotyping the 5HTTLPR

We amplified the polymorphic region of the rhesus monkey serotonin transporter (SLC6A4) promoter⁴² using the following polymerase chain reaction (PCR) primers (forward – 50cagcacctaaccctaatgtccctg30 and reverse – 50gattctggtgccacctagacgccag30) and the PCR conditions described by elsewhere⁴³. Due to lack of DNA or tissue for some subjects, only 226 individuals with behavioral/brain data also had genotype data for the 5HTTLPR measured genotype analysis.

Rhesus Macaque Pedigree

All study subjects that underwent behavioral testing and brain imaging can be linked into a single multi-generation pedigree of more than 1500 individuals. Two of the animals were excluded from the heritability analyses because their paternity was in question. Among the 236 monkeys with phenotype data, there are three full-sibling pairs, 189 half-sibling pairs, 128 third-degree relative pairs, 372 fourth-degree relative pairs, and much larger numbers of more distantly related and unrelated pairs. The number of founders contributing to the pedigree used in this study is relatively large, 348. The largest contribution of any single founder to the phenotyped sample is only 1.67% of total genetic material. The top 50 founders account for 49% of the genetic material of the phenotyped monkeys. The top 201 founders capture 90% of the total genetic material. Among the 238 phenotyped individuals there were 79 different sires. The maximum number of phenotyped study subjects with the same sire is 7, and there are 52 sires that have 3 or fewer offspring in the study group.

Implementation of Voxelwise Quantitative Genetic Analysis

We estimated the heritability of metabolic activity at each voxel measured during FDG-PET scanning using SOLAR⁴⁴, our general computer package for statistical genetic analyses. SOLAR uses a general variance component method making it possible to analyze family-based quantitative data from pedigrees of any size and complexity. Quantitative genetic analysis partitions the observed covariance among related individuals into genetic vs. environmental components. For the simplest univariate case (e.g., a single trait such as total brain volume), the covariance matrix (Ω) in a family (pedigree) of n members has the form $\Omega = 2\Phi\sigma_a^2 + I_n\sigma_e^2$ where Φ is the $n \times n$ kinship matrix for the pedigree, σ_a^2 is the variance in the trait due to additive genetic effects, I_n is the $n \times n$ identity matrix, and σ_e^2 is the variance due to random (unmeasured), individual-specific environmental effects. The basic parameters estimated in this model include the mean, standard deviation, and heritability (h^2) of the voxel-wise metabolic brain activity, where $h^2 = \sigma_a^2 / (\sigma_a^2 + \sigma_e^2)$. Likelihood ratio statistics were used to assess significance of each voxel-specific heritability. The LRT was calculated as twice the difference in likelihoods between a model in which h^2 is estimated versus a model in which h^2 is constrained to zero. Under the null hypothesis, this test statistic is distributed as 50:50 mixture of a chi-square variate with one degree of freedom and a point mass at zero. To ensure that neuroimaging traits conform to the assumptions of normality, an inverse normal transformation was applied. Covariates such as sex, age, and their interactions as well as gray matter probability were included in the mean effects model in each analysis. Because of the large number of voxel-specific analyses required and the large matrix inversions entailed in the likelihood evaluations of this

complex rhesus monkey pedigree, the computational burden was formidable. To minimize analysis time, we therefore employed a specialized parallel version of SOLAR that simultaneously utilized 3,000 processors at SFBR's AT&T Genomics Computing Center.

Supplementary Table 2

Local maxima from Table 1		Location relative to anterior commissure (<i>in mm</i>)			heritability (h^2) of the voxel
Hemisphere	Regions within cluster	x	y	z	
R	dorsal amygdala (CeA/ASTZ region)	12.500	-0.625	-8.750	0.02; $p = 0.454$
	ventral putamen	14.375	-5.625	-8.125	0.13; $p = 0.273$
	superior temporal sulcus (anterior)	18.750	-0.625	-11.250	0.25; $p = 0.086$
	temporopolar cortex	19.375	5.000	-8.125	0.02; $p = 0.459$
L	anterior hippocampus	-12.500	-3.750	-9.375	0.52; $p = 0.001$
	ventral putamen/posterior amygdala	-11.250	-2.500	-8.125	0.18; $p = 0.154$
	mid hippocampus	-15.625	-7.500	-10.625	0.43; $p = 0.003$
	claustrum	-14.375	3.125	-10.000	0.00; $p = 0.500$
	superior temporal sulcus	-18.750	0.625	-8.125	0.00; $p = 0.500$
	hypothalamus	-1.875	-4.375	-6.875	0.28; $p = 0.048$
R	pulvinar	10.625	-15.625	1.250	0.36; $p = 0.007$
crosses midline	intraparietal sulcus (right)	4.375	-27.500	16.875	0.39; $p = 0.031$
	precuneus (left)	-3.125	-29.375	15.000	0.29; $p = 0.058$
	V3 (right)	6.250	-33.750	9.375	0.34; $p = 0.042$
L	V2	-10.000	-28.125	-3.750	0.45; $p = 0.005$
	parietooccipital sulcus	-3.750	-36.875	1.875	0.33; $p = 0.036$
	V1	-13.750	-31.250	-1.875	0.36; $p = 0.016$
R	V2	6.875	-30.625	-2.500	0.49; $p = 0.002$
	V3	11.250	-31.875	-6.875	0.93; $p = 0.000$
R	V1	3.125	-43.750	-3.750	0.50; $p = 0.007$
R	superior temporal sulcus (posterior)	15.625	-25.000	8.750	0.51; $p = 0.007$

Table S2. Heritability of the local maxima within clusters where regional brain metabolism during the NEC challenge was correlated with AT. Data are presented with the hemisphere, brain regions, and the location (in millimeters relative to the anterior commissure). The heritability (h^2) of FDG-PET signal in each of the voxels is also reported. CeA; *amygdala central nucleus*, ASTZ; *amygdalostratial transition zone*.

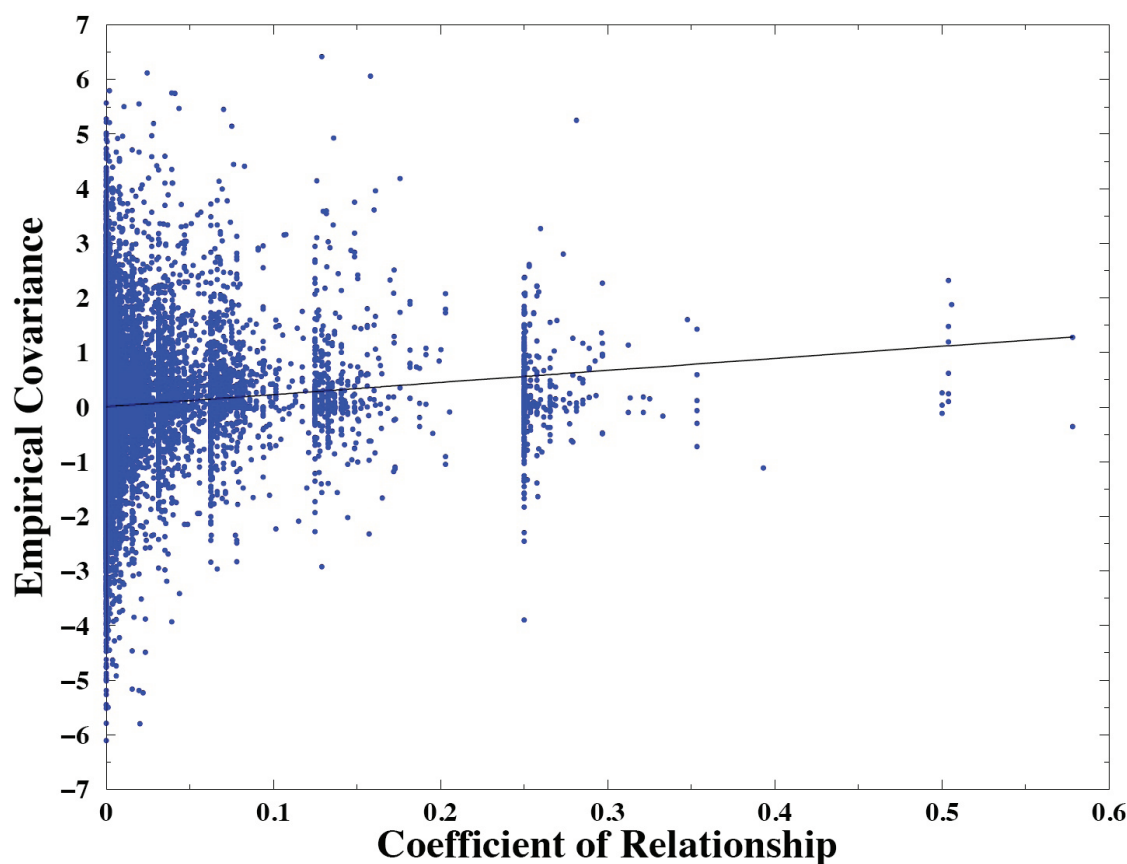


Figure S2. This graph illustrates how covariances between relatives in the most heritable hippocampal voxel provide information on heritability. Each point on the graph represents a pair of animals with imaging data. For each pair, we plot the empirical covariance (defined as $[x_i - \mu_i][x_j - \mu_j]$, where x_i represents the phenotypic measure of the i^{th} monkey and μ_i is its expectation) of hippocampal FDG versus the coefficient of relationship (equal to twice the kinship coefficient). In this figure, 1st order relatives that share ~50% of their genes have a Coefficient of Relationship of 0.5, second degree relatives have a coefficient of 0.25 and third degree relatives have a coefficient of relationship of 0.125.

- 31 Paxinos, G., Huang, X., Petrides, M., and Toga, A., *The rhesus monkey brain in stereotaxic coordinates*, 2nd ed. (Academic Press, San Diego, 2009).
- 32 Jenkinson, M., Bannister, P., Brady, M., and Smith, S., Improved optimization for the robust and accurate linear registration and motion correction of brain images. *Neuroimage* **17**, 825-841 (2002).
- 33 Zhang, Y., Brady, M., and Smith, S., Segmentation of brain MR images through a hidden Markov random field model and the expectation-maximization algorithm. *IEEE Trans Med Imaging* **20**, 45-57 (2001).
- 34 Friston, K. J. et al., Analysis of fMRI time-series revisited. *Neuroimage* **2**, 45-53 (1995).
- 35 Worsley, K. J., Poline, J. B., Friston, K. J., and Evans, A. C., Characterizing the response of PET and fMRI data using multivariate linear models. *Neuroimage* **6**, 305-319 (1997).
- 36 Oakes, T. R. et al., Integrating VBM into the General Linear Model with voxelwise anatomical covariates. *Neuroimage* **34**, 500-508 (2007).
- 37 Ma, L., Worsley, K. J., and Evans, A. C., Variability of spatial location of activation in fMRI and PET CBF images. *Neuroimage* **9**, S178 (1999).
- 38 Christian, B. T. et al., Serotonin transporter binding and genotype in the nonhuman primate brain using [C-11]DASB PET. *Neuroimage* **47**, 1230-1236 (2009).
- 39 Tai, Y. C. et al., Performance evaluation of the microPET P4: a PET system dedicated to animal imaging. *Physics In Medicine And Biology* **46**, 1845-1862 (2001).
- 40 Innis, R. B. et al., Consensus nomenclature for in vivo imaging of reversibly binding radioligands. *Journal of Cerebral Blood Flow and Metabolism* **27**, 1533-1539 (2007).
- 41 Cohen, J and Cohen, P., *Applied multiple regression / correlation analysis for the behavioral sciences*. (Lawrence Erlbaum Associates, Hillsdale, NJ, 1983).
- 42 Lesch, K. P. et al., The 5-HT transporter gene-linked polymorphic region (5-HTTLPR) in evolutionary perspective: alternative biallelic variation in rhesus monkeys. Rapid communication. *J Neural Transm* **104**, 1259-1266 (1997).
- 43 Rogers, J. et al., Mapping of the serotonin transporter locus (SLC6A4) to rhesus chromosome 16 using genetic linkage. *Cytogenet Genome Res* **112**, 341A (2006).
- 44 Almasy, L. and Blangero, J., Multipoint quantitative-trait linkage analysis in general pedigrees. *Am J Hum Genet* **62**, 1198-1211 (1998).